Electron energy-loss spectrum of an electron passing near a locally anisotropic nanotube

D. Taverna,[1] M. Kociak,[1] V. Charbois,[1,*] and L. Henrard[2]
[1]*Laboratoire de Physique des Solides, Associé au CNRS, Bâtiment 510, Université Paris-Sud, 91405, Orsay, France*
[2]*Laboratoire de Physique du Solide, Facultés Universitaires Notre-Dame de la Paix, 61 rue de Bruxelles, 5000 Namur, Belgium*
(Received 17 April 2002; revised manuscript received 1 August 2002; published 30 December 2002)

We have analytically computed the energy-loss probability of a fast electron passing near a locally anisotropic hollow nanotube, in the nonretarded approximation. Numerical simulations have been performed in the low loss (below 50 eV) region, and a good agreement with experimental spatially resolved electron energy-loss spectroscopy results is reported. We also show the importance of the surface coupling effect and of the local anisotropy of the tubes for the plasmonic response, extending the conclusions previously reported for spherical nano-objects.

DOI: 10.1103/PhysRevB.66.235419 PACS number(s): 68.37.Lp, 68.37.Uv, 73.21.−b, 78.67.Ch

I. INTRODUCTION

The discovery of carbon nanotubes[1] opened new fields in physics. Due to their low dimensionality, they attracted the interest of many scientists for possible applications in nanotechnology and, from a more fundamental point of view, they represent an ideal object to experimentally test the validity of models in physics of low dimensions. Besides carbon nanostructures, a considerable effort has been done in the synthesis of non-carbon-based layered nanotubes [e.g., BN (Ref. 2) and WS_2 (Ref. 3)]. The electromagnetic response of these particles requires a dedicated analysis because of their peculiar anisotropy.

On the experimental side, electron energy-loss spectroscopy (EELS) (Ref. 4) is a very well adapted tool to study the dielectric response of nano-objects, especially when combined with the high spatial resolution reached in a scanning transmission electron microscope. The interpretation of the EEL spectra in the 1–50-eV energy range is far from being straightforward, and an adapted theoretical framework is then required. Among others (boundary element method,[5] discrete dipole approximation[6]), the continuum dielectric theory is the most popular approach (see Ref. 7 for a review).

The EELS simulation is based on the knowledge of the dielectric response function of the nanoparticle, defined as the proportionality coefficient between an external exciting potential and the induced one. This dielectric response function in the low loss region (below 50 eV) is the signature of the elementary excitations of valence electrons such as the *interband transition excitations* (excitation of an individual electron from the valence band into the conduction band) and the *plasmon excitations* (collective oscillation modes of the valence electrons). This paper presents an extension of the study of dielectric response of nanoparticles to anisotropic cylindrical hollow nanoparticles. We restrict our work to the nonretarded continuum approach.

At the nanoscale, the contribution to the loss spectra of the surface excitations (the surface plasmons) are of prime importance. If the particle is hollow, the coupling between the electromagnetic modes of the internal and external surface has moreover to be considered. For a very thin shell, the validity of a continuum approach also has to be questioned.

The theoretical study of the excitation of surface plasmon by an external electron dates back to the pioneer work of Ritchie.[8] In the 1980s, several authors[9–11] developed and applied the dielectric model to the spherical geometry in the nonretarded limit. A relativistic approach has been given in Ref. 12. To our knowledge Chu *et al.* have been the first to study the excitation of plasmons by an electron travelling in a cylindrical cavity.[13] Since this problem was treated in several studies,[14–16] as well as the problem of electrons passing perpendicularly to a cylindrical rod.[17,18] Surface plasmon coupling in isotropic hollow nanosphere[19] and nanocylinders[18,20] was also been considered in the past years.

The peculiarity of carbon nanoparticles (and of related objects) is their anisotropy. They can be considered uniaxial particles with their optical axis locally oriented in the radial direction. In order to account for this local anisotropy, the dielectric model was extended to spherical anisotropic nanoparticles[6,21] and tested by comparison with experimental data.[22,23] Here we present a further extension of the dielectric theory to hollow anisotropic nanocylinders for an electron travelling perpendicular to the tube axis. A first qualitative approach at the same problem was given in the literature.[24]

The paper is structured as follows. The analytical calculation is presented in detail in Sec. II. The dielectric response is calculated by expressing in an appropriate basis the electrostatic potential in the different regions of space (Sec. II A) and imposing boundary conditions (Sec. II B). To calculate the energy-loss (II C), we first express in a cylindrical basis the potential of the probe electron (Sec. II C 1), because this determines the induced potential (Sec. II C 2), and because the coefficients of its Fourier expansion are needed to calculate the *probe factor* (Sec. II C 3). All the terms are collected in Sec. II C 3 to give the total energy loss of the electron. Some limit cases of the dielectric response, that give an insight into the peculiar role of coupling and anisotropy, are also evaluated and compared to analogous expressions found in the literature (Sec. II D). Finally, in Sec. III, EELS simulations for WS_2 nanotubes are displayed and compared to experimental data, as well as to analogous simulations in spherical geometry. A detailed analysis of the contributions of the different surface modes to the total loss is also presented.

 ©2002 The American Physical Society

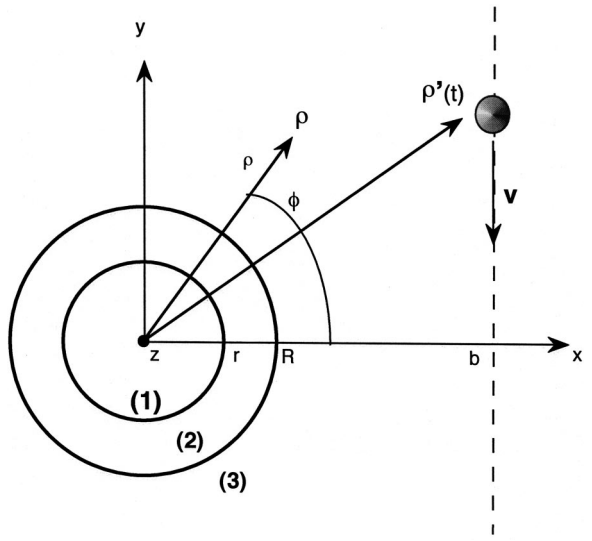

FIG. 1. Geometry of an EELS experiment for a hollow nanotube of internal radius r and external radius R. The electron moves with a speed v along a linear trajectory at distance b (impact parameter) from the particle axis. The positions are expressed in cylindrical coordinates (ρ,θ,z) with the z direction parallel to the tube axis.

II. ANALYTICAL CALCULATION

In this section we present the details of the calculation of the electron energy-loss spectrum of a high-energy electron passing near a locally anisotropic tube. The electron is considered as a nonquantum, nonrelativistic particle, as well as the field it generates. Its trajectory is assumed to be rectilinear and nonperturbed by the interaction with the nanoparticle. This assumption is justified by the small wavelength of the fast electron (energy of the order of 100 keV and $\lambda = 0.02$ Å) as compared to the size of the investigated object and its high energy compared to the energy loss (less than 50 eV). The dielectric response of the particle is considered as local [the local displacement field at point $\mathbf{r}$ depends only on the electric field at the same point, $\mathbf{D}(\mathbf{r})=\overline{\overline{\epsilon}}(\mathbf{r})\mathbf{E}(\mathbf{r})$]. Finally a continuum assumption is made.

First we present the geometry of the modelled experiment and the form of the electrostatic potential. Then a computation of the dielectric response function of a locally anisotropic tube in obtained. Finally, we compute the energy-loss function.

A. Geometry and electrostatic potential

Figure 1 displays the geometry of the modelled experiment. The electron follows a rectilinear uniform trajectory, $\boldsymbol{\rho}'(t)$, parallel to the y axis outside an hollow cylinder. The hollow cylinder has external radius R, an internal radius r and its axis is along z. The *impact parameter* b of the incident electron is defined as the distance between this rectilinear trajectory and the tube axis. A cylindrical coordinates system (ρ,ϕ,z) centered on the tube axis is chosen. We define three regions—the internal region (1), the shell (2), and the external region (3)—in which the nonretarded Maxwell equations have to be solved to determine the potentials.

1. Regions (1) and (3)

In these regions, free of material, the dielectric constant is set equal to the unity for all energy range, and the nonretarded potential verifies the Poisson equation $\nabla^2 V^{(1,3)}=0$. The general solution in cylindrical coordinates is[25]

$$V^{(1,3)}(\rho,\phi,z)=\sum_{m=-\infty}^{+\infty}\int_0^{+\infty} dk R_{m,k}^{(1,3)}(\rho)\cos(kz)e^{im\phi}, \quad (1)$$

with

$$R_{m,k}^{(1,3)}(\rho)=F_{m,k}^{(1,3)}I_m(k\rho)+G_{m,k}^{(1,3)}K_m(k\rho) \quad (2)$$

where I_m and K_m are modified Bessel functions, $F_{m,k}$ and $G_{m,k}$ do not depend on the spatial coordinates, but only on m and k. Thus for region (1),

$$R_{m,k}^{(1)}=F_{m,k}^{(1)}I_m(k\rho) \quad (3)$$

because $K_m(x)$ diverges for $x=0$. For region (3),

$$R_{m,k}^{(3)}=F_{m,k}^{(3)}I_m(k\rho)+G_{m,k}^{(3)}K_m(k\rho), \quad (4)$$

where $F_{m,k}^{(3)}I_m(k\rho)$ describes the applied field and $G_{m,k}^{(3)}K_m(k\rho)$ describes the cylinder response.

2. Region (2)

As already mentioned, due to the lamellar structure of the shell, the dielectric function is endowed with a tensorial character. The anisotropy axis is defined by the direction perpendicular to the basal plane, that is the radial direction for cylindrical particles.

Therefore, the component of the dielectric function in this direction $\epsilon_\parallel$ differs from the in-plane component $\epsilon_\perp$. The nonretarded Maxwell equations lead to

$$\nabla\cdot(\overline{\overline{\epsilon}}\nabla V^{(2)})=0, \quad (5)$$

with

$$\overline{\overline{\epsilon}}=\begin{pmatrix}\epsilon_\parallel & 0 & 0\\ 0 & \epsilon_\perp & 0\\ 0 & 0 & \epsilon_\perp\end{pmatrix}, \quad (6)$$

where the tensor $\overline{\overline{\epsilon}}$ is expressed in the (ρ,ϕ,z) basis (this is the mathematical translation of the concept of local anisotropy). Equation (5) gives [the explicit dependence of $V^{(2)}$ on the spatial coordinates (ρ,ϕ,z) is omitted for clarity].

$$\partial_\rho^2 V^{(2)}+\frac{1}{\rho}\partial_\rho V^{(2)}+\frac{1}{\lambda}\left(\frac{1}{\rho^2}\partial_\phi^2 V^{(2)}+\partial_z^2 V^{(2)}\right)=0, \quad (7)$$

with

$$\lambda=\frac{\epsilon_\parallel(\omega)}{\epsilon_\perp(\omega)}. \quad (8)$$

The solutions can be factorized as in the previous case. The dependence in the ϕ and z variable remains unchanged. On the other hand, the ρ dependence is modified by the anisotropy. The general solution of Eq. (7) gives

$$V^{(2)}=\sum_{m=-\infty}^{+\infty}\int_0^{+\infty}dk[F_{m,k}^{(2)}I_\nu(\zeta)+G_{m,k}^{(2)}K_\nu(\zeta)]\cos(kz)e^{im\phi}, \tag{9}$$

with $\nu=m/\sqrt{\lambda}$ and $\zeta=\rho k/\sqrt{\lambda}$.

B. Dielectric response

In order to obtain the dielectric response function, we compute the coefficients $(F_{m,k}^{(i)},G_{m,k}^{(i)})$ using the boundary conditions at the interfaces region (1)/region (2) ($\rho=r$) and region (2)/region (3) ($\rho=R$):

$$(\mathbf{D}_2-\mathbf{D}_1)\cdot\mathbf{n}_{21}=\sigma=0, \tag{10}$$

$$V^{(1)}(\rho=r,\phi,z)=V^{(2)}(\rho=r,\phi,z); \tag{11}$$

thus

$$\epsilon_\parallel E_\rho^{(2)}(r)-E_\rho^{(1)}(r)=0, \tag{12}$$

$$V^{(1)}(\rho=r)=V^{(2)}(\rho=r), \tag{13}$$

and similar relations for the interface (2/3).

We then obtain four linearly independent equations for the five unknowns $(F_{m,k}^{(1)},F_{m,k}^{(2)},F_{m,k}^{(3)},G_{m,k}^{(2)},G_{m,k}^{(3)})$. The decomposition of the potential of the probe electron gives the $F_{m,k}^{(3)}$ coefficient (see Sec. II C) and all the other unknowns can be expressed as a function of this coefficient. The coefficient of the induced potential, $G_{m,k}^{(3)}$ then defines the dielectric response of the nanocylinder:

$$\alpha_{m,k}(\omega)=-\frac{G_{m,k}^{(3)}}{F_{m,k}^{(3)}}. \tag{14}$$

For convenience, we define the dimensionless quantities $\xi=kr/\sqrt{\lambda}$, $W=kR/\sqrt{\lambda}$, $x=kr$, and $X=kR$. After some algebra, we express

$$\alpha_{m,k}(\omega)=\frac{A+B}{C+D}, \tag{15}$$

with (the symbol $'$ means the derivative with respect to the argument of the Bessel function)

$$A=(A_1+A_2)I_m'(x), \tag{16a}$$

$$A_1=\lambda I_m'(X)[I_\nu(W)K_\nu(\xi)-I_\nu(\xi)K_\nu(W)], \tag{16b}$$

$$A_2=\epsilon_\parallel\sqrt{\lambda}I_m(X)[I_\nu(\xi)K_\nu'(W)-I_\nu'(W)K_\nu(\xi)], \tag{16c}$$

$$B=(B_1+B_2)\epsilon_\parallel I_m(x), \tag{17a}$$

$$B_1=\sqrt{\lambda}I_m'(X)[I_\nu'(\xi)K_\nu(W)-I_\nu(W)K_\nu'(\xi)], \tag{17b}$$

$$B_2=\epsilon_\parallel I_m(X)[I_\nu'(W)K_\nu'(\xi)-I_\nu'(\xi)K_\nu'(W)], \tag{17c}$$

$$C=(C_1+C_2), \tag{18a}$$

$$C_1=\lambda I_m'(x)K_m'(X)[I_\nu(W)K_\nu(\xi)-I_\nu(\xi)K_\nu(W)], \tag{18b}$$

$$C_2=\epsilon_\parallel^2 I_m(x)K_m(X)[I_\nu'(W)K_\nu'(\xi)-I_\nu'(\xi)K_\nu'(W)], \tag{18c}$$

$$D=\sqrt{\lambda}\epsilon_\parallel(D_1+D_2), \tag{19a}$$

$$D_1=I_m(x)K_m'(X)[I_\nu'(\xi)K_\nu(W)-I_\nu(W)K_\nu'(\xi)], \tag{19b}$$

$$D_2=I_m'(x)K_m(X)[I_\nu(\xi)K_\nu'(W)-I_\nu'(W)K_\nu(\xi)]. \tag{19c}$$

Note that the dielectric response depends on Bessel functions with both complex arguments and complex order. In any case, $\alpha_{m,k}(\omega)$ depends only on the characteristics of the particle (inner and outer radius, and dielectric tensor of the corresponding lamellar material).

C. Energy losses

For computing the energy losses, we follow the classical procedure,[7,10] i.e., we compute the time Fourier transform of the exciting potential (due to the probe electron). We then deduce the frequency dependent induced potential. The total energy loss is given by (q is the charge of the electron)

$$W(b)=-qv\int_{-\infty}^{\infty}\mathbf{E}_{ind}[\boldsymbol{\rho}=\boldsymbol{\rho}'(t),t]\cdot\mathbf{u}_y dt$$

$$=\int_0^{\infty}d\hbar\omega\hbar\omega\frac{dP}{dE}(\omega,b), \tag{20}$$

where dP/dE is the energy-loss probability by energy unit.

1. Potential created by a point charge moving along a rectilinear uniform in a cylindrical coordinates basis

In this section, following Ref. 18, we express the potential due to the probe electron in a basis adapted to cylindrical symmetry. Let us assume that an electron is moving along a rectilinear uniform trajectory with velocity **v** (see Fig. 1). At each time (the quasistatic approximation), the potential $V(\boldsymbol{\rho},\boldsymbol{\rho}')$ created at point $\boldsymbol{\rho}$ by the electron placed in $\boldsymbol{\rho}'(t)$ can be decomposed in cylindrical components as[25]

$$V(\boldsymbol{\rho},\boldsymbol{\rho}')=\frac{q}{2\pi^2\epsilon_0}\sum_{m=-\infty}^{+\infty}\int_0^{+\infty}dke^{im(\phi-\phi')}$$

$$\times\cos[k(z-z')]I_m(k\rho)K_m(k\rho'), \tag{21}$$

where ϵ_0 is permittivity of vacuum. Note that the previous expression is valid for $\rho<\rho'(t)$ (we are interested in the potential in the region between the nanotube and the fast electron) The charge q follows the trajectory

$$\boldsymbol{\rho}'(t)=[\rho'(t),\phi'(t),z'(t)]$$

$$=[\sqrt{b^2+v^2t^2},\arctan(vt/b),0]. \tag{22}$$

One can then rewrite the potential as a function of its Fourier components,

$$V(\boldsymbol{\rho},\boldsymbol{\rho}')=\frac{q}{4\pi^3\epsilon_0}\sum_{m=-\infty}^{+\infty}\int_0^{+\infty}dk\int_{-\infty}^{+\infty}d\omega\quad e^{im\phi}\times\cos[kz]I_m(k\rho)C_{m,k}(\omega)e^{-i\omega t}\tag{23}$$

with

$$C_{m,k}(\omega)=\int_{-\infty}^{+\infty}dtK_m[k\rho'(t)]e^{-im\phi'(t)}e^{i\omega t}\tag{24}$$

The evaluation of this last expression gives[18]

$$C_{m,k}(\omega)=\frac{\pi}{v}\frac{e^{-b\sqrt{k^2+(\omega/v)^2}}}{\sqrt{k^2+\left(\frac{\omega}{v}\right)^2}}\left(\frac{\sqrt{k^2+\left(\frac{\omega}{v}\right)^2}+\frac{\omega}{v}}{k}\right)^m.\tag{25}$$

2. Applied and induced potentials

One can now evaluate the induced potential. We supposed that the induced potential is linearly dependent on the applied one, and their Fourier coefficients are related by expression (14). Therefore, we find

$$V_{ind}(\boldsymbol{\rho},\boldsymbol{\rho}')=\frac{-q}{4\pi^3\epsilon_0}\sum_{m=-\infty}^{+\infty}\int_0^{+\infty}dk\int_{-\infty}^{+\infty}d\omega\quad e^{im\phi}\times\cos[kz]I_m(k\rho)\alpha_{m,k}(\omega)C_{m,k}(\omega)e^{-i\omega t}.\tag{26}$$

We finally have all the elements necessary to the calculation of the energy loss.

3. Computation of the energy loss

As the electron trajectory is along the y direction, from Eq. (20) and with $\mathbf{E}_{ind}=\nabla_{\boldsymbol{\rho}=\boldsymbol{\rho}'}V_{ind}(\boldsymbol{\rho},t)=\partial_{y=y(t)}V_{ind}(\boldsymbol{\rho},t)=(1/v)\partial_t V_{ind}(\boldsymbol{\rho},t)$.

$$W(b)=\frac{-q^2v}{4\pi^3\epsilon_0}\sum_{m=-\infty}^{+\infty}\int_0^{+\infty}dk\int_{-\infty}^{+\infty}d\omega\int_{-\infty}^{+\infty}dt\times\alpha_{m,k}(\omega)C_{m,k}(\omega)\frac{1}{v}\partial_t[K_m(k\rho(t))e^{im\phi(t)}]e^{-i\omega t}.\tag{27}$$

We integrate by parts and, as K_m goes asymptotically to zero, we find the limit

$$\lim_{t\to\pm\infty}K_m[kr(t)]e^{im\phi(t)}=\lim_{t\to\pm\infty}K_m(k\sqrt{b^2+v^2t^2})e^{im\arctan(vt/b)}=0.\tag{28}$$

We obtain the expression

$$W(b)=\frac{-q^2v}{4\pi^3\epsilon_0}\sum_{m=-\infty}^{+\infty}\int_0^{+\infty}dk\int_{-\infty}^{+\infty}d\omega\int_{-\infty}^{+\infty}dt\times\alpha_{m,k}(\omega)C_{m,k}(\omega)\frac{i\omega}{v}\{K_m[kr(t)]e^{im\phi(t)}\}e^{-i\omega t}.\tag{29}$$

The integration over the time was already computed: it is the complex conjugate of the coefficient $C_{m,k}(\omega)$, which is real. Then

$$W(b)=\frac{-q^2}{4\pi^3\epsilon_0}\sum_{m=-\infty}^{+\infty}\int_0^{+\infty}dk\int_{-\infty}^{+\infty}d\omega\alpha_{m,k}(\omega)C_{m,k}^2(\omega)i\omega\tag{30}$$

In order to obtain the expression of the energy-loss probability per energy unit we have to compare the last expression with Eq. (20). To this end, we write Eq. (30) as an integration over positive frequencies and, by using the relations $\alpha_{m,k}(\omega)=-\alpha_{m,k}(-\omega)$ and $C_{m,k}(\omega,b)=C_{-m,k}(-\omega,b)$, we obtain

$$\frac{dP}{dE}(\omega,b)=\frac{q^2}{2\pi^3\epsilon_0\hbar^2}\times\sum_{m=-\infty}^{+\infty}\int_0^{+\infty}dk\,\mathrm{Im}[\alpha_{m,k}(\omega)]C_{m,k}^2(\omega,b)\tag{31}$$

with $C_{m,k}(\omega,b)$ given by Eq. (25) and $\alpha_{m,k}(\omega)$ by Eq. (15).

We now have the expression for the energy loss of an electron passing aloof a locally anisotropic tube at the distance (impact parameter) b. This classical expression is valid for a single inelastic-scattering event, it does not account for multiple excitation processes, neither for energy gains by de-excitation transitions. Note that this energy-loss spectrum is a sum over the momentum along the tube axis (k) and the transferred azimuthal momentum (m) of a product of two functions. The second one, $C_{m,k}^2(\omega,b)$, is directly related to the probe electron field, and does not depend on the particle characteristics (provide it is cylindrical), while the first one is the dielectric response function, that characterizes the particle. Note also that, due to the exponential dependence in expression (25), the kinematic factor $C_{m,k}(\omega,b)$ acts as a low-k and low-ω filter. In particular, we find that the integration over k in the previous expression (31) runs up to a cutoff k, depending on the impact parameter b. In any case, this classical treatment demands $ka\ll 1$, where a is the interatomic distance.

Maxima of $P(\omega,b)$ are directly related to those of $\mathrm{Im}[\alpha(\omega)]$, and then to the plasmon normal mode of the nanotube. For isotropic compounds (planar slab,[27] sphere,[19,28] or cylinder[27,29]) the polarizability or response function present two poles for real dielectric function and the dispersion of those modes can be studied as a function of kd (plane), l and r/R (sphere), or m and $k_z d$ (cylinders). For anisotropic materials, α is imaginary even for real dielectric function, because the factor λ could be imaginary for real $\overline{\overline{\epsilon}}$.

The number of modes is then not well defined (or normal modes does not exist anymore) and the apparent number of modes depends on the width of the resonance in $\epsilon(\omega)$. This has been already noted for a plane,[30] sphere,[22,31] and a cylinder for $k_z=0$.[32]

D. Some limits

Here we give some limits of Eq. (31), in order to compare to previous works on the energy loss of a filled isotropic tube[18] and on the dielectric response of anisotropic tube in the $k\to 0$ limit.[6] In this limit we further examined the effect of the *radius ratio* $\Theta=r/R$ on the coupling of electromagnetic surface modes, by analyzing the dielectric response when $\Theta\to 1$ and $\Theta\to 0$. $r\to 0$ and $k\to\infty$ are also obtained and compared to the dielectric response of a thick anisotropic slab.

1. Energy loss for a filled isotropic tube

In their work, Bertsch *et al.*[18] did not explicitly use a dielectric response/probe decomposition of the energy loss. However, they deduced a very similar form. Translating formula (19) of Ref. 18 to our convention (in particular, CGS to MSKA unit systems), the energy-loss probability per energy unit for an electron travelling perpendicular to an isotropic filled tube, at a distance b from its axis, is expressed by Bertsch *et al.*[18] as

$$\frac{dP}{dE}(\omega,b)=\frac{2q^2}{4\pi\epsilon_0\pi^2\hbar^2}\sum_m\int_0^{+\infty}dk I_m(kR)I_m'(kR)kR \times \mathrm{Im}[\Pi_{m,k}(\omega)]C_{m,k}^2(\omega,b), \tag{32}$$

with

$$\Pi_{m,k}(\omega)=\frac{1-\epsilon}{\epsilon+(\epsilon-1)K_m(kR)I_m'(kR)kR}. \tag{33}$$

Then we can identify the dielectric response function of Eq. (31) to the previous expression if

$$\lim_{\substack{r\to 0,\\ \epsilon_\perp=\epsilon_\parallel=\epsilon}}\alpha_m(k)=kRI_m(kR)I_m'(kR)\Pi_{m,k}(\omega). \tag{34}$$

To reach these limits, we remember that for $r\to 0$, and when $m\neq 0$,

$$I_m(x)\sim\frac{1}{\Gamma(m+1)}\left(\frac{x}{2}\right)^m, \tag{35}$$

$$K_m(x)\sim\frac{\Gamma(m)}{2}\left(\frac{2}{x}\right)^m, \tag{36}$$

while for $m=0$, $I_m(x)\to 1$ and $K_m(x)\sim-\ln(x)$. For all values of m, we find

$$\alpha_{m,k}(\omega)\sim\frac{(1-\epsilon)I_m(kR)I_m'(kR)}{\epsilon K_m(kR)I_m'(kR)-I_m(kR)K_m'(kR)}, \tag{37}$$

and using the identity $xI_m(x)'K_m(x)-xI_m(x)K_m(x)'=1$, we retrieve Bertsch *et al.*'s expression.

2. Dielectric response for a hollow locally anisotropic cylinder in the limit $k\to 0$

Taking into account the anisotropy, Henrard and Lambin[6] calculated, in the $k=0$ limit, the polarizability per unit length of a hollow cylinder (inner and outer radii respectively r and R),

$$\gamma_m(\omega)\sim 4\pi\epsilon_0 R^{2m}\frac{(\epsilon_\parallel\epsilon_\perp-1)(1-\Theta^{2\nu})}{(\sqrt{\epsilon_\parallel\epsilon_\perp}-1)^2\Theta^{2\nu}-(\sqrt{\epsilon_\parallel\epsilon_\perp}+1)^2}, \tag{38}$$

with $\Theta=r/R$ and $\nu=m/\sqrt{\lambda}$. The expression refers to $k=0$ and is valid only for $m\neq 0$ (if both k and m are strictly equal to zero, there is no momentum transfer and the cylinder is not polarisable by an external charge). By again using approximations (35) and (36) we find the expression of the dielectric response of the anisotropic tube,

$$\alpha_{m,k}(\omega)\sim\frac{2}{\Gamma(m)\Gamma(m+1)}\left(\frac{kR}{2}\right)^{2m} \times\frac{(\epsilon_\parallel\epsilon_\perp-1)(1-\Theta^{2\nu})}{(\sqrt{\epsilon_\parallel\epsilon_\perp}-1)^2\Theta^{2\nu}-(\sqrt{\epsilon_\parallel\epsilon_\perp}+1)^2}, \tag{39}$$

showing the dependence on the radius ratio previewed by Henrard and Lambin, but with a prefactor proportional to the mth power of the dimensionless factor kR, as expected for a multipolar polarizability. Thus we have found that our general expression can be reduced to limits previously published in the literature.

Moreover, we analyze Eq. (39) in the two limit cases of the radius ratio Θ. When $\Theta\to 1$, Eq. (39) reads

$$\alpha_{m,k}(\omega)\sim\frac{2}{\Gamma(m)\Gamma(m+1)}\times\left(\frac{kR}{2}\right)^{2m}m(1-\Theta)\left(\epsilon_\perp-\frac{1}{\epsilon_\parallel}\right). \tag{40}$$

For long wavelengths and large Θ, the dielectric response of an anisotropic cylinder is then similar to that of a slab in a regime where the two surface electromagnetic excitations are strongly coupled. Such limit has also been found for anisotropic spheres.[33] The importance of the local anisotropy is emphasized by the fact that, in this limit, $\alpha(\omega)$ is not invariant by inversion of the parallel and perpendicular components of the dielectric tensor.

On the other hand, when $\Theta\to 0$, Eq. (39) gives

$$\alpha_{m,k}(\omega)\sim\frac{2}{\Gamma(m)\Gamma(m+1)}\left(\frac{kR}{2}\right)^{2m}\frac{\sqrt{\epsilon_\parallel\epsilon_\perp}-1}{\sqrt{\epsilon_\parallel\epsilon_\perp}+1}, \tag{41}$$

and we retrieve the dielectric response of an anisotropic slab in the weak coupling regime, i.e., the surface response function of a semi-infinite anisotropic crystal.[35] Therefore, for small values of k but nonzero m, the coupling regime between the plasmons of the inner and the outer surfaces of the

tube is strongly sensitive to the radius ratio. If k is small and $m=0$, the dielectric response can be approximated for all Θ by

$$\alpha_{0,k}(\omega)\sim 2\left(\frac{kR}{2}\right)^2(1-\Theta^2)(\epsilon_\perp-1), \tag{42}$$

showing no dispersion of the electromagnetic modes as a function of Θ. We note that the last expression is similar to that of a thin anisotropic slab in the strong coupling regime (as expected when all the components of the momentum-transfer are very small). In particular, we note that expression (42) is similar to Eq. (40) for what concerns the $\epsilon_\perp$, but the $\epsilon_\parallel$ dependence has disappeared. In Ref. 33, it was shown that the $\epsilon_\perp$ dependence is related to the antisymmetric (radial) mode, where the $\epsilon_\parallel$ dependence is related to the symmetric (tangential) mode. For $m=0$ and very small k, the radial mode is characterized by an uniform and opposite charge distribution on the inner and outer surfaces and then to an absence of external induced field. Therefore, in these conditions, such a radial mode cannot be excited by an external electron. Finally, as $\Theta<1$, at large m Eq. (39) can again be approximated by Eq. (41), and we also find a dependence on $(\sqrt{\epsilon_\parallel\epsilon_\perp}-1)/(\sqrt{\epsilon_\parallel\epsilon_\perp}+1)$ typical of the weak coupling regime.

3. Dielectric response for a hollow locally anisotropic cylinder in the limit $k\to\infty$

Another interesting limit is that of the very large values of k $(k\gg 1/R,1/r)$, where the Bessel functions have the following asymptotic behavior[26]:

$$K_m(x)\sim\sqrt{\frac{\pi}{2x}}e^{-x}, \tag{43}$$

$$I_m(x)\sim\frac{e^x}{\sqrt{2\pi x}}, \tag{44}$$

and the dielectric response of the locally anisotropic tube can be expressed as

$$\alpha_{m,k}(\omega)\sim\frac{e^{2kR}}{\pi}\left(\frac{\sqrt{\epsilon_\parallel\epsilon_\perp}-1}{\sqrt{\epsilon_\parallel\epsilon_\perp}+1}\right). \tag{45}$$

Then, independently of m and Θ, for small wavelengths we find the dielectric response of an anisotropic cylinder is similar to the one of a weakly coupled anisotropic slab. When computing the energy-loss spectrum, the exponential divergent factor in the response function [Eq. (15)] is compensated for by the probe term [Eq. (31)], that vanishes exponentially with kb (in a nonpenetrating geometry $b\geqslant R$) and, like in the sphere case,[6] acts as a k-momentum filter.

III. NUMERICAL SIMULATIONS

We now turn to numerical simulations. The computations are based on the analytical expression of the energy-loss probability [Eq. (31)], depending on the probe factor [Eq. (25)] and on the dielectric response [Eq. (15)]. They are performed by using the software MATHEMATICA (by Wolfram Research Inc.), allowing the evaluation of complex Bessel functions of complex order.

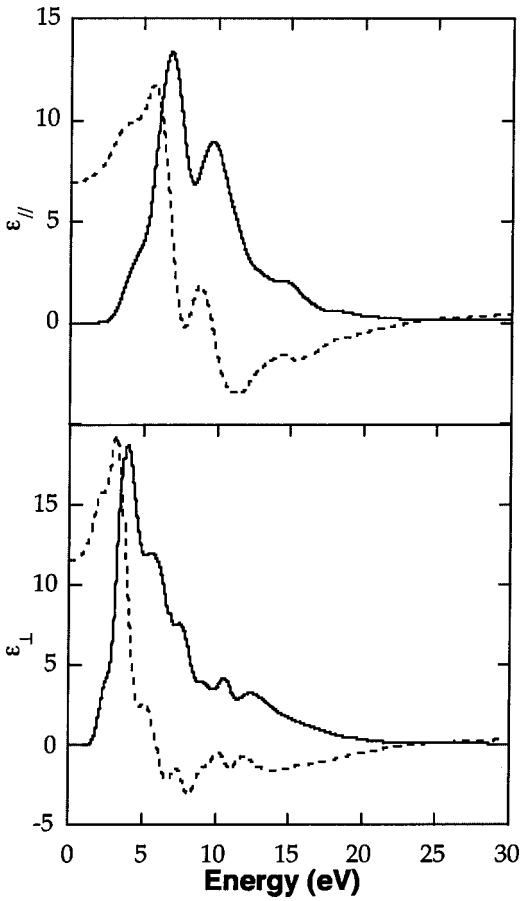

FIG. 2. *Ab initio* computations of the dielectric constant of WS_2. Dotted lines: real parts; solid lines: imaginary parts. Top: parallel component; bottom: perpendicular one.

In the present dielectric formalism, the internal (r) and external (R) radii and the impact parameter (b) are parameters that can be varied at will, allowing the study of nanotubes with different structures and the simulation of *line spectra*.[36] The case of WS_2 nanotubes was chosen for the numerical simulation, because they were shown to be a good experimental example for the study of the surface plasmon coupling in hollow anisotropic cylindrical nanoparticles.[33] The dielectric tensor of lamellar WS_2, which was used as input data in the following calculations, is displayed in Fig. 2. It was computed *ab initio* in the local density approximation (LDA)[37] using the commercial software CASTEP (by Molecular Simulations Inc.).

Figure 3 displays the simulated results as well as their experimental counterparts, for two tubes of different radius ratios (thick tube $R=20.5$ nm and $r=10.5$ nm$\Rightarrow\Theta=0.51$; thin tube $R=6.7$ nm and $r=6$ nm$\Rightarrow\Theta=0.90$) in a geometry where the probe is at grazing incidence (see Ref. 33 for more details on the experimental setup). The simulations are in

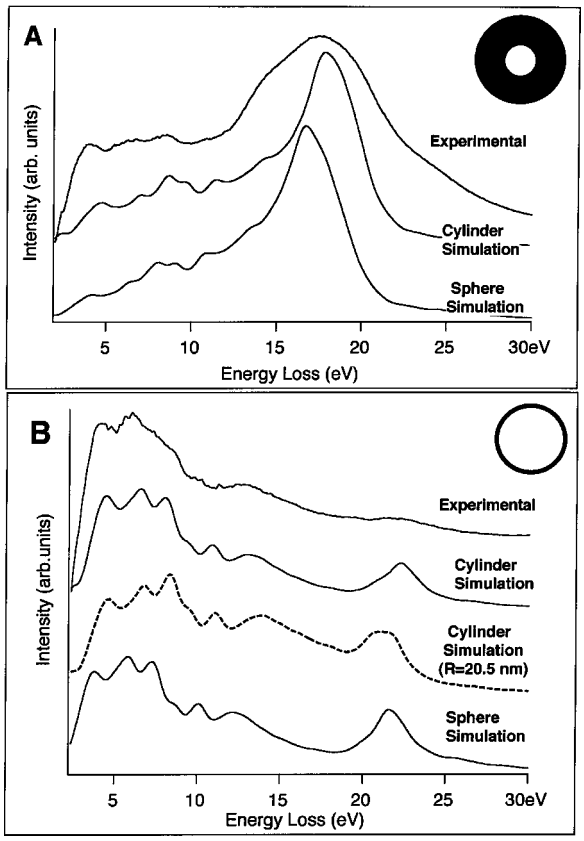

FIG. 3. Comparison of simulations for WS_2 nanotubes and nanospheres and experimental spectra of WS_2 nanotubes. **A**: the thick shelled tube ($R=20.5$ nm, $r=10.5$ nm$\Rightarrow\Theta=0.51$; $b=21.5$ nm). **B**: thin shelled tube with $\Theta=0.90$; solid lines: experimental spectra, and simulations in cylindrical and spherical geometries for a tube of $R=6.7$ nm, $r=6$ nm with $b=7.7$ nm; dashed line: simulation in cylindrical geometry for a tube with $R=20.5$ nm and $b=21.5$ nm.

very good agreement with the experimental results, i.e., the differences between the two situations (radius ratio $\Theta=0.51$ and 0.90) are accurately reproduced. The only discrepancy between the experimental data and the simulation is the intensity of the 22-eV mode in Fig. 3(b) (it appears as a small bump on experimental data). This peak is directly related to $\epsilon_{\parallel}$ (see later). The lack of accuracy in the LDA calculation for out-of-plane excitations in layered system explains this problem.

For these calculations, the contributions of the terms up to $m=7$ and $k=14/b$ ($=0.7$ and 1.8 nm^{-1} respectively for the thick and the thin tubes) have been considered for the loss spectra [Eq. (31)]. Larger transfer momenta have been found to make negligible contributions. Also note that these cutoff values have to be compared to the experimental limit imposed by the collection angle at the entry of the spectrometer (≈ 3 nm^{-1}).

The calculations performed for a locally anisotropic cylinder and for a nanosphere with the same radius ratio (see Ref. 21 for the theory for the spherical geometry) are surprisingly close together. However, in the simulation for thick tube the low energy modes are slightly more pronounced (Fig. 3). In contrast, the high energy mode of the thin tube is less intense in the cylindrical model than in the spherical one. For both values of the radius ratio, however, the cylindrical geometry presents peaks slightly shifted toward higher energy as compared to the spherical geometry and the modeling in cylindrical geometry fits the experimental data slightly better. These similarities rely on the fact that the excitation along the circumference of a tube is similar to that along the circumference of a sphere and to the fact that only the mode of small k significantly contributes to the loss of nanocylinders. In Ref. 33, this argument was evoked to justify an interpretation of WS_2 nanotube experimental loss spectra based on simulation in the spherical geometry. The present simulations dedicated to cylindrical geometry then fully justify *a posteriori* our previous conclusions.

In Ref. 33 we attributed the striking difference between the spectra obtained for different radius ratios to the regime of the strong and weak coupling between electromagnetic surface modes. In order to better illustrate the prime importance of the radius ratio on the EEL spectra, in Fig. 3B we display a simulated curve for $\Theta=0.90$ but with the same R and b than for Fig. 3A (dashed curve). The shape of the energy loss is very similar between tubes with same Θ but different absolute value of r and R, and the differences in the relative intensities can be attributed to the increase of the contribution weight of high momentum order modes as the external radius increases (see below). For the thick tube, the two surfaces do not couple, and the spectrum depends on the geometric average of the perpendicular and parallel component of the dielectric tensor [see the analytical form of the limit, Eqs. (41) and (45)]. At the opposite, for the thin tube, electromagnetic surface excitations do couple, leading to a clear splitting of the spectrum into two parts. The low-energy part is related to $\epsilon_{\perp}$, and is similar to tangential (or symmetric) excitation of a virtual isotropic nanocylinder with a dielectric function $\epsilon(\omega)=\epsilon_{\perp}(\omega)$. The high-energy peak is related to $\epsilon_{\parallel}$, and to the radial (or antisymmetric) excitation of a virtual isotropic cylinder with a dielectric function $\epsilon(\omega)=\epsilon_{\parallel}(\omega)$. See Ref. 19 for more details on radial and tangential modes of isotropic nanoparticles.

From the previous discussion, it appears that both the anisotropy and the hollow character of the cylindrical nanoparticles are of prime importance. A more systematic study of the variation of the EELS data as a function of the radius ratio was presented elsewhere for carbon nanotubes.[34] It is also worth noting that, for a nanocylinder, the $m=0$ mode is excitable by an external electron for $k\neq 0$, as opposed to the spherical geometry case where the $l=0$ mode is silent for a non-penetrating electron.

We now analyze the contribution to the total spectrum of the different terms of Eq. (31). Figure 4 gives the m decomposition of the total loss spectra for thick [Fig. 4(a)] and thin [Fig. 4(b)] nanotubes, obtained by integrating over k. The decreasing contribution of high multipolar order m allows a convergence of the sum. For thin tube modes $m=0$ and 1 mainly contribute to the total spectra, while for thick tubes modes up to $m=7$ have to be included. The kinematic factor

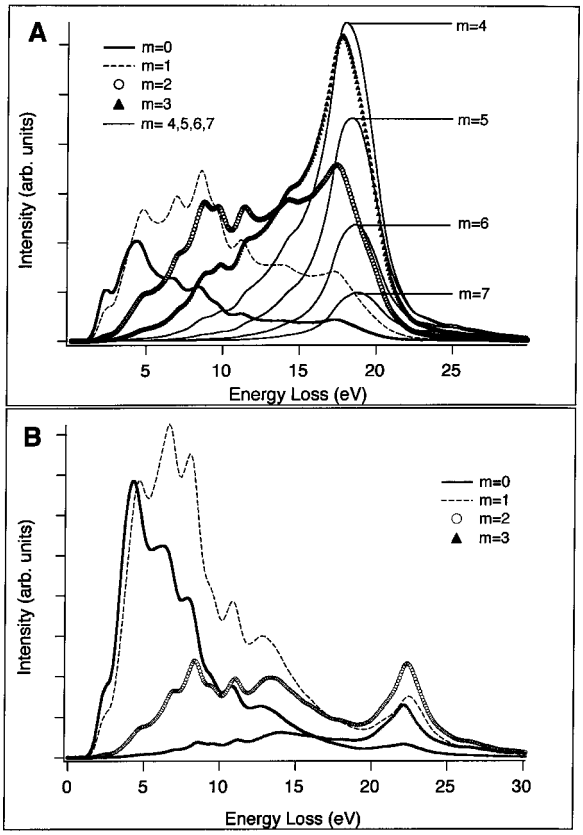

FIG. 4. Contributions of the different multipolar (m) excitation to the total spectrum of thick (**A**) and thin (**B**) WS_2 nanotubes. Thick solid line: mode $m=0$. Dashed line: mode $m=1$. Empty circles: $m=2$. Triangles: $m=3$. Thin solid lines: higher multipolar excitations (m varying from 4 to 7). See Fig. 3 for r, R, and b.

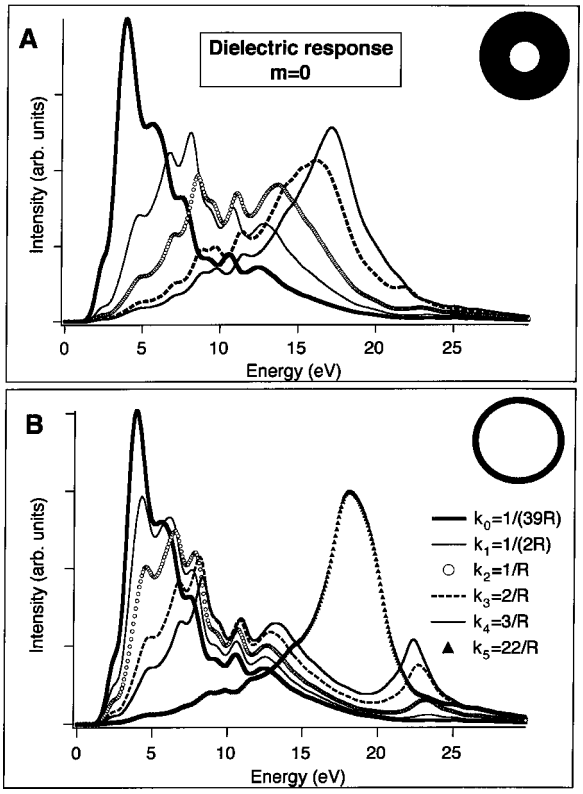

FIG. 5. Dispersion of the dielectric response of the thick (**A**) and thin (**B**) nanotubes as a function of the momentum transfer k, for $m=0$. See Fig. 3 for the definition of r, R, and b. The curves have been normalized with respect to their integrated area. **A**: the normalization constant for the thick tube are: $n(K_0)=2\times10^{-5}$; $n(K_1)=0.007$; $n(K_2)=0.031$; $n(K_3)=0.300$; $n(K_4)=2.381$. **B**: the normalization constant for the thin tube are $n(K_0)=7\times10^{-7}$; $n(K_1)=0.002$; $n(K_2)=0.013$; $n(K_3)=0.148$; $n(K_4)=1.391$; $n(K_5)=2\times10^{17}$.

[Eq. (25)] being identical in both cases, this difference is due to the response function [Eq. (15)]. This shape variation of the response function is dominated by the width of the shell, then by the possibility of surface excitation coupling (see below).

In Fig. 5, we analyze the k dispersion of the $m=0$ mode for thick [Fig. 5(a)] and thin [Fig. 5(b)] nanotubes. To compensate for the k divergence of the dielectric response, the curves are normalized to the same area. The curves represent the response function [Eq. (15)] and are then set free of the filtering effect of the probe factor. For both shell thickness, the $k=0$ mode presents the same aspect, following the analytical limit we found [Eq. (42)]. In Fig. 5(a), we emphasize the rapid dispersion of the $m=0$ mode for thick tubes. It is striking to note that, for large k, the $m=0$ mode is very similar to the high m mode [Fig. 4(a)]. On the other hand, in the thin shell case, the dispersion is less pronounced and the convergence is only reached for very large k transfer [Fig. 5(b), solid triangles].

In Fig. 6 the response functions of Fig. 5 are multiplied by the probe factor in order to show the role of the probe factor as a low-k filter. Due to the exponential k divergence of the dielectric response the excitations at very small k modes show a weaker probability, but this effect is compensated for by the probe factor, and beyond $k=1/(2R)$ the high-k modes become less and less intense. The exponential ω decay of the probe factor leads to a variation of the relative intensities of the modes at a fixed k, as compared to the intensities dis-

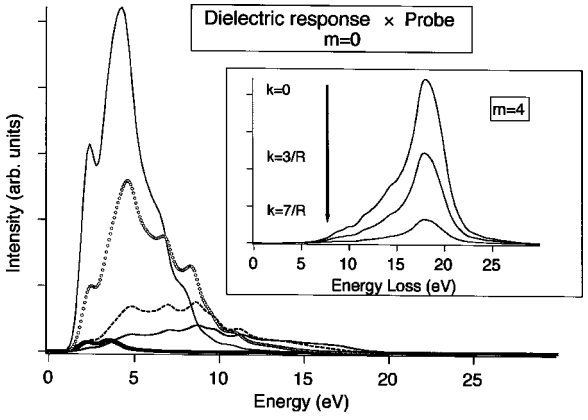

FIG. 6. Excitation probability of the $m=0$ mode for various momentum transfer k. See Fig. 5 for the exact k values and Fig. 3 for r, R, and b parameters. Inset: same for the $m=4$ mode.

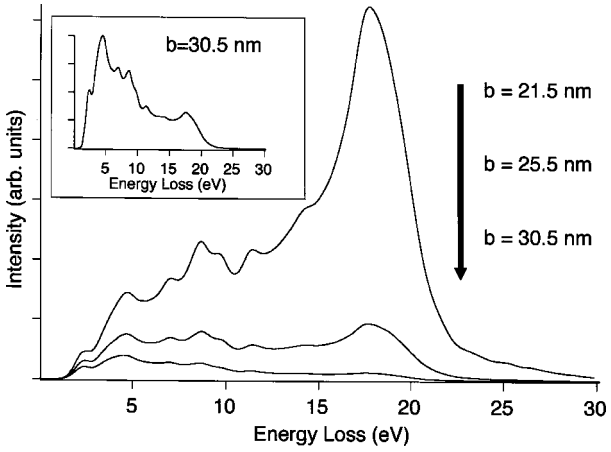

FIG. 7. Loss spectra of a thick tube (see Fig. 3 for parameters) as a function of the impact parameter b. Inset: rescaled $b = 30.5$ nm spectrum.

played in the dielectric response [Fig. 5(a)]. The same spectra for $m=4$ are shown in the inset. As previously explained, the high-m modes do not disperse and already present a weak coupling limit type of spectra (see the end of Sec. II D 2). This point has been already noted for the isotropic filled cylinders in the pioneer work of Kliewer and Fuchs.[27]

In order to qualitatively explain such m and k dependence of the spectra, we come back to the simplest surface coupling system, the planar film.[27] The coupling in a planar geometry depends on the $k_p d$ parameter (d being the thickness of the film and k_p the momentum transfer parallel to the surface): for small $k_p d$, the two surface modes are symmetric and antisymmetric modes, denoting a strongly coupled system, where at large $k_p d$ only a single degenerated surface mode is present. This is the weak coupling limit. Keeping in mind that the probe factor [$C_{m,k}$, Eq.(25), in cylindrical geometry] acts as a low pass filter in k (or k_p), only modes with k (k_p)$<k_{max}$ contribute to the total spectra. If $k_{max}d$ is small (thin film) only strong coupling terms contribute to the total spectra. As soon as d increases, the large $k_p d$ term dominates the total spectra and low coupling limit is reached.[27]

In the present cylindrical geometry, the coupling parameter $k_p d$ has to be replaced by kR and $m(1-\Theta)$. The signature of the strong coupling then appears in terms where both m and k are small. On the other hand, the similarity between the shapes of the dielectric response at large m or large k, is due to the weak coupling regime that is reached for high total momentum transfers in both cases. However, a formal and quantitative discussion of the coupling with respect to m and k is made very cumbersome due to the complexity of expression (15). However, in the $\Theta \to 0$ limit [Eqs. (41) and (45)], the $\sqrt{\epsilon_\perp \epsilon_\parallel}$ dependence indicates a weak coupling between surfaces, while the $\Theta \to 1$ and $k \to 0$ limit presents two distinct surface modes, characteristic of a strong coupling.

As a last discussion point, we would like to show the impact parameter dependence of the EELS spectra of WS_2 cylinders. Figure 7 shows this dependence for the thick tube example. Of course, as expected, the loss probability drops rapidly with the impact parameter. A very striking point is the radical change of the shape of the loss spectra with b (the $b=30.5$ nm spectrum is rescaled in the inset for a better comparison). Such a strong dependence of the loss spectra is related to the strong m and k dispersive behaviors of the nanotube. If the electron beam is at grazing incidence, large m and k modes are excited. As the electron probe moves away from the nanoparticle, the low m and k modes become predominant and the large dispersion explains the change in the spectral shape. The same effect (but less pronounced) has been previously reported for planar interfaces[38] and for spheres.[22]

IV. CONCLUSION

In this paper, we have presented an analytical calculation of the electron energy-loss spectrum of a hollow and locally anisotropic nanotube, when the probe is not crossing the tube. The continuum dielectric approach has been followed in the nonretarded approximation.

The previous analysis of the energy loss of multilayer nanotubes relied on an isotropic model[18] or on an anisotropic nanosphere model.[22,33] But the recent and rapid development of the production capability of anisotropic nanocylinders [made of C, BN,[2] and WS_2 (Ref. 3)] as new classes of materials increase the number and the quality of EELS experimental data available, and made a modelization adapted to the cylindrical anisotropic cylinder necessary.

Here we have presented a numerical application of the formalism to the energy loss of WS_2 nanotubes in the 5–50-eV range, and a comparison with recent experimental data has been shown to be a success. In a parallel paper,[34] we also applied the present formalism to an interpretation of carbon nanotubes electron energy-loss data.

We have also explored analytic limit cases of the general expression. For example, small and large radius ratio limits have been considered, as well as the small momentum transfer limit. We have numerically analyzed the surface plasmon coupling for thin and thick WS_2 nanotubes for such limits.

We should also emphasize that, in the present formalism, the probe factor [Eq. (25)] and the response function of the nanoparticle [Eq. (15)] are distinct in the total loss expression [Eq. (31)]. More complex systems of cylindrical symmetry, such as bundle of nanotubes, could then be possible to handle by adapting the response function term only.

ACKNOWLEDGMENT

The authors are grateful to O. Stéphan for stimulating discussions and to Ph. Lambin and C. Colliex for their support during this work. We thank E. Sandŕe for providing us the *ab initio* dielectric function of WS_2. D.T. was supported by EU-TMR ''Ultra-Hard Materials'' and JST/CNRS ICORP Nanotubolites Project. L.H. was supported by the Belgian National Fund (FNRS). This work was also partly funded by the Belgian Interuniversity Research Project on quantum size effects in nanostructured materials (PAI-UAP P5-1). The authors acknowledge support from the french-belgian cooperation program Tournesol 2002.

*Now at CEA/Service de Physique de l'Etat Condensé, 91191 Gif sur Yvette cedex, France
[1] S. Iijima, Nature (London) **354**, 65 (1991).
[2] A. Loiseau, F. Willaime, N. Demoncy, G. Hug, and H. Pascard, Phys. Rev. Lett. **76**, 4737 (1996).
[3] R. Tenne, L. Margulis, M. Genut, and G. Hodes, Nature (London) **360**, 444 (1992).
[4] H. Cohen, T. Maniv, R. Tenne, Y.R. Hacohen, O. Stéphan, and C. Colliex, Phys. Rev. Lett. **80**, 782 (1998).
[5] F.J. Garcia de Abajo and A. Howie, Phys. Rev. Lett. **80**, 5180 (1998).
[6] L. Henrard and Ph. Lambin, J. Phys. B **29**, 5127 (1996).
[7] Z.L. Wang, Micron **27**, 265 (1996).
[8] R.H. Ritchie, Phys. Rev. **106**, 874 (1957).
[9] T.L. Ferell and P.M. Echenique, Phys. Rev. Lett. **55**, 1526 (1985).
[10] P.M. Echenique, A. Howie, and D.J. Weathley, Philos. Mag. B **56**, 335 (1987).
[11] D. Ugarte, C. Colliex, and P. Trebbia, Phys. Rev. B **45**, 4332 (1992).
[12] F.J. Garcia de Abajo, Phys. Rev. B **59**, 3095 (1999).
[13] Y.T. Chu, R.J. Warmack, R.H. Ritchie, J.W. Little, R.S. Becker, and T.L. Ferrell, Part. Accel. **16**, 13 (1984).
[14] C.R. Walsh, Philos. Mag. A **59**, 227 (1989).
[15] N. Zabala, A. Rivacoba, and P. Echenique, Surf. Sci. **209**, 465 (1989).
[16] N.R. Arista and M.A. Fuentes, Phys. Rev. B **63**, 165401 (2001).
[17] A. Rivacoba, P. Apell, and N. Zabala, Nucl. Instrum. Methods Phys. Res. B **96**, 470 (1995).
[18] G.F. Bertsch, H. Esbensen, and B.W. Reed, Phys. Rev. B **58**, 14 031 (1998).
[19] Ph. Lambin, A.A. Lucas, and J.P. Vigneron, Phys. Rev. B **46**, 1794 (1992).
[20] U. Schroter and A. Dereux, Phys. Rev. B **64**, 125420 (2001).
[21] A.A. Lucas, L. Henrard, and P. Lambin, Phys. Rev. B **49**, 2888 (1994).
[22] M. Kociak, L. Henrard, O. Stéphan, K. Suenaga, and C. Colliex, Phys. Rev. B **61**, 13 936 (2000).
[23] T. Stockli, J.M. Bonard, A. Chatelain, Z.L. Wang, and P. Stadelmann, Phys. Rev. B **61**, 5751 (2000).
[24] T. Stoeckli, Z.L. Wang, J.M. Bonard, P. Stadelmann, and A. Chatelain, Philos. Mag. B **79**, 1531 (1999).
[25] J. D. Jackson, *Classical Electrodynamic* (Wiley, New York, 1998).
[26] *Handbook of Mathematical functions*, edited by M. Abramowitz and I. A. Segun (Dover, New York, 1972).
[27] K.L. Kliewer and R. Fuchs, Adv. Chem. Phys. **XXVII**, 355 (1974).
[28] L. Henrard, O. Stephan, and C. Colliex, Synth. Met. **103**, 2502 (1999).
[29] L. Henrard, P. Senet, Ph. Lambin, and A.A. Lucas, Fullerene Sci. Technol. **4**, 133 (1996).
[30] Ph. Lambin, P. Senet, A. Castiaux, and L. Philippe, J. Phys. I **3**, 1417 (1993).
[31] L. Henrard, O. Stephan, M. Kociak, C. Colliex, and Ph. Lambin, J. Electron Spectrosc. Relat. Phenom. **219**, 114 (2001).
[32] E. Balan, F. Mauri, C. Lemaire, Ch. Brouder, A.M. Saiita, and B. Devouard, Phys. Rev. Lett. **89**, 177401 (2002).
[33] M. Kociak, O. Stéphan, L. Henrard, V. Charbois, A. Rothschild, R. Tenne, and C. Colliex, Phys. Rev. Lett. **87**, 075501 (2001).
[34] O. Stéphan, D. Taverna, M. Kociak, K. Suenaga, L. Henrard, and C. Colliex, Phys. Rev. B **66**, 155422 (2002).
[35] A.A. Lucas and J.P. Vigneron, Solid State Commun. **49**, 327 (1984).
[36] C. Jeanguillaume and C. Colliex, Ultramicroscopy **28**, 252 (1989).
[37] M.C. Payne, M.T. Teter, D.C. Allan, T.A. Arias, and J.D. Joannopoulos, Rev. Mod. Phys. **64**, 1045 (1992).
[38] P. Moreau, N. Brun, C.A. Walsh, C. Colliex, and A. Howie, Phys. Rev. B **56**, 6774 (1997).